Interference effects: A key to understanding forbidden Raman scattering by LO phonons in GaAs

José Menéndez and Manuel Cardona
Max-Planck-Institut für Festkörperforschung, Heisenbergstrasse 1, D-7000 Stuttgart 80, Federal Republic of Germany
(Received 22 October 1984)

We show that the contributions of intrinsic and impurity-induced forbidden LO-phonon Raman scattering in GaAs can be quantitatively separated by investigating interference effects between allowed and forbidden LO-phonon scattering. We perform a new calculation of impurity-induced scattering and determine the resonance profile for GaAs near the $E_0+\Delta_0$ gap. Comparison with experiment shows that impurity-induced scattering plays a dominant role. Absolute values of the Raman efficiencies are estimated and compared with experiment.

I. INTRODUCTION

Since the first observations[1,2] of dipole-forbidden Raman scattering by LO phonons, this phenomenon has been reported for a number of semiconducting materials. (For reviews, see Refs. 3 and 4.) "Forbidden" scattering by iractive LO phonons can be seen for photon energies near electronic transitions with incident ($\hat{\mathbf{e}}_L$) and scattered ($\hat{\mathbf{e}}_S$) polarizations parallel to each other. This scattering does not follow the selection rules imposed on the Raman tensor by the symmetry of the Γ-point phonons. Different mechanisms have been proposed. Pinczuk and Burstein[2] showed that when the scattering volume is close to the sample surface, electric fields due to band bending can produce forbidden LO-phonon scattering.

In the case where surface electric fields can be ignored because the scattering occurs in the bulk, it was shown[5] that forbidden LO-phonon scattering may arise from intraband matrix elements of the Fröhlich electron-phonon interaction if the dependence of these matrix elements on the phonon wave vector $\mathbf{q}$ is taken into account. For a small-q ($q\equiv|\mathbf{q}|$) intraband transition, the symmetry of the two electronic states connected by the Fröhlich Hamiltonian remains unchanged. Thus, the Raman tensor has the same symmetry as the dielectric tensor, i.e., it is diagonal for transitions near $\mathbf{k}=\mathbf{0}$ in cubic semiconductors. A diagonal Raman tensor can explain the observed selection rule $\hat{\mathbf{e}}_L\|\hat{\mathbf{e}}_S$. However, in the dipole approximation (the limit in which the phonon wave vector $\mathbf{q}$ vanishes), the electron and hole contributions cancel exactly, and the intraband Fröhlich matrix elements do not produce Raman scattering.

The phonon wave vector $\mathbf{q}$ is actually very small in a first-order Raman process, because crystal-momentum conservation implies $\mathbf{q}=\mathbf{k}_L-\mathbf{k}_S$, where $\mathbf{k}_L$ ($\mathbf{k}_S$) is the wave vector of the incident (scattered) photon. Nevertheless, it is not exactly zero. Hamilton[5] and Martin and Damen[6] showed that for $\mathbf{q}\neq\mathbf{0}$ one obtains a strongly resonant Raman efficiency proportional to q^2. On the other hand, if the intermediate electronic states are excitons bound to impurities,[7] one also has nonzero matrix elements of the Fröhlich interaction for all phonon $\mathbf{q}$ vectors, leading to a forbidden Raman efficiency which, in contrast to the previous case, does not depend explicitly on the scattering wave vector $\mathbf{q}$.

An additional scattering mechanism involving impurities was proposed by Gogolin and Rashba.[8] Here, a higher-order process is considered, in which a *free* exciton[9] scatters twice: once due to the electron-phonon interaction and again due to the electron-impurity interaction. The large momentum transfers which take place in the impurity-scattering process enhance the scattering cross sections despite the high order of perturbation theory (fourth) involved.

Efforts to separate intrinsic from extrinsic (impurity-related) contributions to the forbidden scattering have been based on calculations of the efficiencies for the different mechanisms proposed,[10,11] or in an experimental search for the explicit q dependence of the Raman polarizability predicted in Martin's theory.[6,10] This q dependence has been qualitatively found for very pure CdS samples by Permogorov and Reznitsky,[12] who showed that the forbidden Raman signal for backscattering (large $\mathbf{q}$ transfer) is stronger than for forward scattering (small $\mathbf{q}$ transfer). The situation is much less clear in III-V—compound semiconductors. Most of the experiments were performed at gaps higher than the fundamental one, where forward scattering is impossible and the method of Ref. 12 cannot be applied. The only estimation of absolute efficiencies has been made by Trommer and Cardona for GaAs.[11] These authors show that the intrinsic mechanism is important, but their calculation is based on the quasistatic approximation and is not conclusive.

In this paper we show how recent work[13] on interference between allowed and forbidden LO-phonon scattering can be used to separate different sources of forbidden scattering. The effect is demonstrated at the $E_0+\Delta_0$ gap of GaAs, nearly 1.85 eV at 100 K. At this frequency the penetration depth of the light is greater than 3500 Å, and we can neglect surface-electric-field effects like those discussed by Pinczuk and Burstein.[1] Moreover, no *bound*-exciton states exist near the $E_0+\Delta_0$ gap, so we are left with only two possible mechanisms for forbidden LO-phonon scattering: the intrinsic intraband process pro-

posed by Martin,[6,10] possibly with some excitonic enhancement, and the impurity-assisted scattering of the type discussed by Gogolin and Rashba.[8]

Our procedure is based on the fact that the Raman tensors for allowed scattering and for intrinsic (**q**-induced) forbidden scattering must be added *before* squaring for calculating the Raman efficiency, whereas the tensor for (extrinsic) impurity-induced forbidden scattering must be added to the allowed contribution *after* squaring. This follows from the fact that the final states (LO phonons) for allowed and for **q**-induced forbidden scattering are the same, while in the case of impurity-induced scattering different final states, corresponding to a broad distribution of **q** vectors, are obtained.

Under these conditions, in the backscattering configuration on the (001) face, theory predicts that the Raman efficiency for $\hat{e}_L||\hat{e}_S||[110]$ is different than for $\hat{e}_L||\hat{e}_S||[1\bar{1}0]$ whenever intrinsic forbidden scattering is present, but takes the same value for both polarizations when the observed forbidden scattering is entirely induced by impurities. We fit the scattering efficiencies measured as a function of laser frequency with expressions which allow a determination of the relative strength of the two forbidden mechanisms. The results show that intrinsic forbidden scattering only plays a significant role in high-purity samples, and suggest that most of the forbidden scattering seen in commercial semiconductors is induced by impurities. Knowing the proportion of intrinsic scattering, we can compare the measured absolute efficiencies with the theoretical calculation. The agreement is rather good.

The remainder of the paper is organized as follows: In Sec. II we discuss the experimental setup and the procedure to determine the sample orientation. The experimental results are presented in Sec. III. In Sec. IV we review the theory of first-order Raman scattering and give expressions for the Raman polarizabilities, including signs that are relevant to this work. A new calculation of impurity-induced scattering is introduced, the details of which are relegated to the Appendix. Finally, in Sec. V, we evaluate the theoretical resonant profiles and compare them to experiment.

II. EXPERIMENTAL SETUP AND PROCEDURE

Two samples were used in our experiments:

(a) An n-type 50-μm-thick layer grown by liquid-phase epitaxy on a GaAs(001) substrate.[14] Electrical measurements at 77 K yield $\rho=8.7\ \Omega\,\mathrm{cm}$, $\mu=100.000\ \mathrm{cm^2/V\,sec}$, and $N_D-N_A=10^{13}\ \mathrm{cm^{-3}}$. The estimated amount of impurities is $N_A+N_D\sim 6\times 10^{14}\ \mathrm{cm^{-3}}$.

(b) Czochralski-grown (Wacker Chemitronics GmbH, D-8000 München, Federal Republic of Germany) with $N_D+N_A\sim 10^{16}\ \mathrm{cm^{-3}}$.

We call x, y, and z the [100], [010], and [001] directions, respectively. x' denotes [110] and y' denotes $[1\bar{1}0]$. The [110] and $[1\bar{1}0]$ directions are physically inequivalent, although the labeling [110] and $[1\bar{1}0]$ depends on the choice of coordinates.

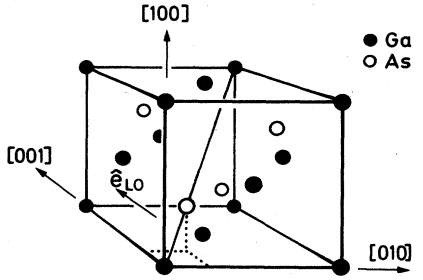

FIG. 1. Cubic cell of GaAs showing the choice of coordinates used in the present work. The unit vector $\hat{e}_{LO}$ characterizes the relative atomic displacements in the LO-phonon mode measured in Raman scattering.

In this paper we choose (Fig. 1) the Ga atom to be at the origin, and the As atom at $(a_0/4)(1,1,1)$. With this convention the $(\bar{1}\bar{1}1)$ plane (parallel to [110]) is Ga-terminated. Preferential etching of the (001) face with HNO_3 or CrO_3/HF produces rectangular pyramidal structures whose faces have been shown to be {111} planes.[15] Because Ga is less reactive than As, Ga-terminated (111) faces develop more easily than As-terminated ones. This means that the longest sides of the pyramids are parallel to [110], allowing an inequivocal orientation of the sample.

For backscattering at the (001) face, the allowed LO-phonon Raman scattering tensor for a zinc-blende material is given (via a deformation-potential interaction) by

$$\overleftrightarrow{R}_{DP}=\begin{bmatrix} 0 & a_{DP} & 0 \\ a_{DP} & 0 & 0 \\ 0 & 0 & 0 \end{bmatrix}. \tag{1}$$

In addition, the forbidden LO-phonon Raman scattering tensor is given (via the Fröhlich interaction) by

$$\overleftrightarrow{R}_{F}=\begin{bmatrix} a_F & 0 & 0 \\ 0 & a_F & 0 \\ 0 & 0 & a_F \end{bmatrix}. \tag{2}$$

The scattering efficiency is therefore proportional to

$$\frac{dS}{d\Omega}$$

$$\propto \begin{cases} |a_F+a_{DP}|^2 & \text{for the } z(x',x')\bar{z} \text{ configuration}, \quad (3a) \\ |a_F-a_{DP}|^2 & \text{for the } z(y',y')\bar{z} \text{ configuration}, \quad (3b) \\ |a_F|^2 & \text{for the } z(x,x)\bar{z} \text{ configuration}. \quad (3c) \end{cases}$$

The difference between $z(x',x')z$ and $z(y',y')\bar{z}$ configurations arises from the fact that we have added $\overleftrightarrow{R}_{DP}$ and $\overleftrightarrow{R}_F$ *before* squaring. This corresponds to the case of intrinsic forbidden LO-phonon Raman scattering. If the forbidden LO-phonon Raman scattering tensor is induced by impurities, we must add the allowed and forbidden contributions *after* squaring. Thus we obtain the same result for

$z(x',x')\bar{z}$ and $z(y',y')\bar{z}$. To check this experimentally, we cut three rectangular slabs from each sample and glued them with silver paste to a cold finger placed in an evacuated Dewar and maintained in contact with liquid nitrogen. The vertical axes corresponded to the [110], [$1\bar{1}0$], and [100] directions, respectively, so that we could measure the $z(x',x')\bar{z}$, $z(y',y')\bar{z}$, and $z(x,x)\bar{z}$ configurations by simply shifting the Dewar horizontally.

A jet-stream dye laser operated with DCM (Ref. 13) (Spectra-Physics) was used to excite the spectra. The dye was pumped with all the lines of a cw Ar^+ laser (5 W). We worked in the frequency range 1.8–2.0 eV, close to the $E_0+\Delta_0$ gap of GaAs. This gap, between the second-highest valence band Γ_7 and the lowest conduction band Γ_6, is the spin-orbit partner of the fundamental gap E_0. The light was focused onto the sample by means of a cylindrical lens, keeping the power density below 100 W/cm^2. The scattered light was analyzed with a Jarrell-Ash 1-m double monochromator equipped with holographic gratings, and detected with an RCA 31034 photomultiplier by photon counting.

In Raman experiments using photon-counting electronics, one measures the scattered-photon rate R_S, which, *inside* the scattering medium, is related to the scattering cross section by[16]

$$\frac{dR_S}{d\Omega}=\frac{I_L}{\hbar\omega_L}\frac{d\sigma}{d\Omega}\ , \tag{4}$$

where ω_L is the incident-photon frequency and I_L is the laser irradiance (power per area). For solids, the cross section $d\sigma/d\Omega$ is proportional to the scattering volume V. Hence it is customary to define a scattering efficiency per unit length and unit solid angle such that

$$\frac{dS}{d\Omega}=\frac{1}{V}\frac{d\sigma}{d\Omega}$$
$$=\frac{\omega_S^3\omega_L}{c^4}\frac{\hbar}{2v_cM^*\Omega_{\rm ph}}\frac{n_S}{n_L}|\hat{\mathbf{e}}_S\cdot\overleftrightarrow{\mathbf{R}}\cdot\hat{\mathbf{e}}_L|^2[1+n(\Omega_{\rm ph})]\ , \tag{5}$$

where ω_S is the scattered-photon frequency, c the speed of light in vacuum, v_c the volume of the primitive cell, $M^*=(M_{\rm Ga}^{-1}+M_{\rm As}^{-1})^{-1}$, the reduced mass of the unit cell, $\Omega_{\rm ph}$ the phonon frequency, $n(\Omega_{\rm ph})$ the phonon occupation factor, n_L (n_S) the refractive index, and $\hat{\mathbf{e}}_L$ ($\hat{\mathbf{e}}_S$) the polarization vector for the incident (scattered) light. Equation (5) defines the Raman tensor $\overleftrightarrow{\mathbf{R}}$, whose independent components are called "Raman polarizabilities."

The final expression for the measured scattering rate *outside* the crystal is given by[16]

$$R_S'=\left\{\frac{T_ST_LP_L'\omega_S^3[n(\Omega_{\rm ph})+1]}{(\alpha_L+\alpha_S)n_Sn_LM^*\Omega_{\rm ph}v_c}\right\}\frac{\Delta\Omega'}{2c^4}|\hat{\mathbf{e}}_S\cdot\overleftrightarrow{\mathbf{R}}\cdot\hat{\mathbf{e}}_L|^2\ , \tag{6}$$

where P_L' is the incident laser power, T_S and T_L the power-transmission coefficients ($T=1-r$, where r is the reflectivity), and $\Delta\Omega'$ the collection solid angle *outside* the crystal. α_L (α_S) are the absorption coefficients at the incident (scattered) frequency.

Equation (6) must be used to obtain absolute values of the Raman tensor by the sample-substitution method.[3] We have used silicon as a reference. For the Raman polarizability (the independent component of $\overleftrightarrow{\mathbf{R}}$), we use $|a|\sim 40$ Å^2 for $\hbar\omega_L=1.85$ eV.[17] The experimental scattering rates R_S' are obtained from the area of the measured Raman peaks. Comparing the results for Si and GaAs, the Raman polarizability of GaAs can be deduced by applying the term in curly brackets in Eq. (6) as a correction factor. We used $\alpha=3.0\times10^4$ cm^{-1} for GaAs (Refs. 18 and 19) and $\alpha=1.4\times10^3$ cm^{-1} for Si (Ref. 20). Additional data were taken from Aspnes and Studna.[21]

III. RESULTS

Figures 2 and 3 show the results obtained for both samples measured. We give the values of the square of the Raman tensor contracted with the polarization vectors. These values are different for the $z(x',x')\bar{z}$ and $z(y',y')\bar{z}$ configurations, thus confirming that at least part of the forbidden scattering indeed interferes with the allowed contribution. However, the interference is weaker for the bulk commercial sample (Fig. 3), which has a larger amount of impurities. Notice also in this case that the forbidden scattering is much stronger (by approximately a factor of 5).

IV. THEORY

A. First-order Raman scattering by phonons

The most strongly resonant of the six diagrams contributing to Stokes first-order Raman scattering is shown in Fig. 4(a). A virtual exciton (electron-hole pair) is created by annihilation of the incoming photon $\hbar\omega_L$. The exciton is scattered via electron-phonon interaction, creating (Stokes case, Fig. 4) or absorbing a phonon $\hbar\Omega_{\rm ph}$. The scattered photon is produced by recombination of the virtual exciton.

The electron-phonon interaction can be separated into a long- and a short-range part:[22]

$$H_{e\rm L}=H_F+H_{\rm DP}\ . \tag{7}$$

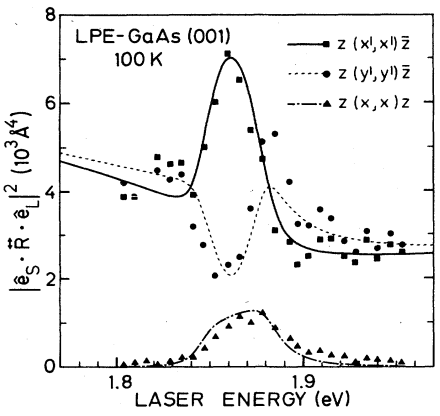

FIG. 2. Measured Raman polarizability for three scattering configurations near the $E_0+\Delta_0$ gap of liquid-phase-epitaxy GaAs. The lines represent the fit using Eqs. (20) and (21).

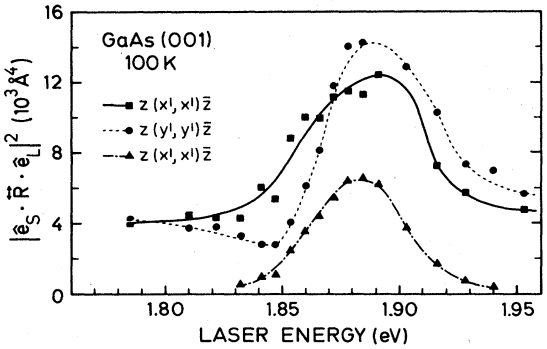

FIG. 3. Same as Fig. 2 for a commercial GaAs sample ($n \sim 10^{16}$ cm^{-3}). The lines are drawn as a guide to the eye.

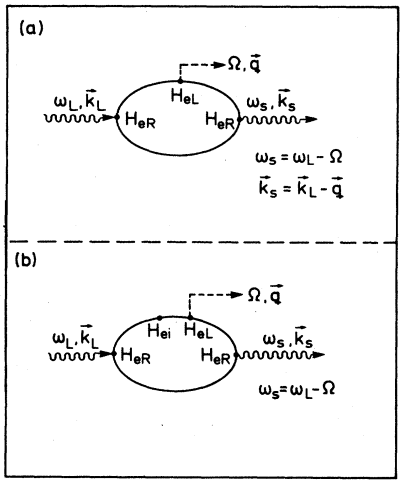

FIG. 4. Typical diagrams for Raman scattering by phonons. H_{eR} (H_{eL}) is the electron-radiation (-phonon) interaction. (a) First-order Raman scattering. (b) Impurity-induced Raman scattering. H_{ei} is the electron-impurity Hamiltonian.

The long-range part H_F is the Fröhlich interaction, which is induced by the electric field created by longitudinal phonons in polar materials. It is zero in covalent semiconductors such as Si and Ge. For LO phonons near the center of the Brillouin zone (those which participate in the Raman process), H_F is given by[22]

$$H_F = -\frac{iC_F}{q^2 V^{1/2}}(\mathbf{q}\cdot\hat{\mathbf{e}}_{\rm LO})(a^\dagger_{-\mathbf{q}} + a_{\mathbf{q}})e^{i\mathbf{q}\cdot\mathbf{r}} . \tag{8}$$

Here, V is the crystal volume, and C_F is the Fröhlich constant given by

$$C_F = \frac{e_{\rm T}}{\epsilon_\infty \Omega_{\rm LO}}\left|\left[\frac{8\pi^2 e^2 \hbar\Omega_{\rm LO}}{M^* v_c}\right]^{1/2}\right| , \tag{9a}$$

where $e_{\rm T}$ is the transverse dynamical charge of the *cation*, $\hbar\Omega_{\rm LO}$ the LO-phonon energy, e the free-electron charge, and ϵ_∞ the high-frequency dielectric constant, related to $e_{\rm T}$ by

$$\epsilon_\infty = \epsilon_0 - \frac{4\pi e_{\rm T}^2}{M^* v_c \Omega_{\rm LO}^2}\frac{\epsilon_0}{\epsilon_\infty} , \tag{9b}$$

where ϵ_0 is the low-frequency dielectric constant. Note that according to Eq. (9) the sign of C_F is determined by the sign of $e_{\rm T}$.

The unit vector $\hat{\mathbf{e}}_{\rm LO}$ in Eq. (8) is related to the relative sublattice displacement $\mathbf{u}_{\rm rel}$ by

$$\mathbf{u}_{\rm rel} = \mathbf{u}_{\rm As} - \mathbf{u}_{\rm Ga} = \left[\frac{\hbar}{2\Omega_{\rm LO} N M^*}\right]^{1/2}(a^\dagger_{-\mathbf{q}} + a_{\mathbf{q}})e^{i\mathbf{q}\cdot\mathbf{r}}\hat{\mathbf{e}}_{\rm LO} , \tag{10}$$

where N is the number of primitive cells in the crystal, $a^\dagger$ (a) are phonon creation (destruction) operators, and $\hat{\mathbf{e}}_{\rm LO}$ is a unit polarization vector.

The short-range part of the electron-phonon interaction is the deformation-potential interaction, given by[23]

$$H_{\rm DP} = \mathbf{V}(\mathbf{r})\cdot\mathbf{u}_{\rm rel} , \tag{11}$$

where $\langle n,\mathbf{k}\,|\,\mathbf{V}(\mathbf{r})\,|\,n,\mathbf{k}\rangle$ is the shift of the band state $|\,n,\mathbf{k}\rangle$ per unit relative displacement of the sublattices.

The relevant quantity in the microscopic evaluation of the Raman tensor is given by the matrix element W_{fi}:

$$W_{fi} = \sum_{\lambda_1,\lambda_2}\frac{\langle 0;S,1\,|\,H_{eR}(\mathbf{e}_S)\,|\,\lambda_2\rangle\langle\lambda_2\,|\,H_{eL}\,|\,\lambda_1\rangle\langle\lambda_1\,|\,H_{eR}(\mathbf{e}_L)\,|\,0;L,0\rangle}{(E_{\lambda_2}-E_{0,i})(E_{\lambda_1}-E_{0,i})} , \tag{12}$$

where $|\,0,L,0\rangle$ is the ground electronic state with a photon in the incident state L and zero phonons, etc., and λ_1,λ_2 run over all intermediate states. In terms of W_{fi}, the Raman tensor is given by

$$\hat{\mathbf{e}}_S\cdot\vec{\mathbf{R}}\cdot\hat{\mathbf{e}}_L = \frac{1}{\omega_L}\frac{n_S n_L}{2\pi}\left[\frac{2M^*\Omega_{\rm LO} V v_c}{\hbar^3}\right]^{1/2} W_{fi} . \tag{13}$$

For Si and Ge, H_{eL} becomes $H_{\rm DP}$, and the Raman tensor has only one independent component. Its expression is given in Eq. (1) for backscattering at the (001) face ($\mathbf{x}||[100]$, $\mathbf{y}||[010]$). The frequency dependence of $a_{\rm DP}$ has been studied in great detail.[3] For GaAs, an approximate expression for this Raman polarizability (deformation-potential contribution) has been given in Ref. 24 (also see Ref. 3) in terms of critical points:

$$a_{\rm DP} = A_1\left\{-g(x_0) + \frac{4E_0}{\Delta_0}\left[f(x_0) - \left[\frac{E_0}{E_0+\Delta_0}\right]^{3/2} f(x_{0s})\right]\right\} + A_2\left[\frac{1}{1-x_1^2} + \left[\frac{E_1}{E_1+\Delta_1}\right]^2\frac{1}{1-x_{1s}^2}\right] + A_3 . \tag{14}$$

The meaning of the symbols is the same as in Ref. 24. Note that a_{DP} resonates strongly at the E_0 gap, whereas it has a weak singularity at $E_0+\Delta_0$. At this gap the resonance is weak because H_{DP} has no diagonal matrix elements at Γ_6 and Γ_7. The real and imaginary parts of a_{DP} near $E_0+\Delta_0$ are shown in Fig. 3 of Ref. 13.

The sign of a_{DP}, relevant for this work, depends on the definition adopted for $\hat{e}_{LO}$. For phonon vibrations along the z axis, $\hat{e}_{LO}$ may be chosen as either (0,0,1) or (0,0,−1). Both conventions are permitted, but one must use the same definition in H_{DP} and in H_F. With the convention of Fig. 1, the real and imaginary parts of a_{DP} are *positive*[3,25] near the $E_0+\Delta_0$ gap of GaAs.

In the case of polar semiconductors, the contribution of H_F must be considered together with that of H_{DP} to calculate the scattering efficiency. Two different terms arise: The interband matrix elements of H_F, the so-called electro-optic contribution,[3] leads to a Raman tensor which is isomorphic with the deformation-potential tensor, Eq. (1). On the other hand, in the approximation of vanishing phonon wave vector (dipole approximation), the intraband matrix elements of H_F do not contribute to the scattering efficiency. However, for the real case of small but finite phonon wave vector, the intraband matrix elements produce Raman scattering which resonates very strongly near critical points. For the $E_0+\Delta_0$ gap of GaAs, this "forbidden" tensor is diagonal [Eq. (2)]. The calculation of the a_F used in Eq. (2) is quite straightforward.[10,26] The result is, choosing $\hat{e}_{LO}$ as in Fig. 1,

$$a_F=\frac{q}{12\pi}\left[\frac{e}{m\hbar}\right]^2\frac{C_F}{\hbar\Omega_{LO}}\left[\frac{1}{\omega_L}\right]^2\left[\frac{\omega_L}{\omega_S}\right]^{1/2}(4v_c\mu M^*)^{1/2}\left[\frac{2P^2}{3}\right](s_e-s_h)F(\omega_L)\ . \tag{15}$$

Here, e and m are the free-electron charge and mass, respectively, $\mu^{-1}=m_e^{-1}+m_h^{-1}$, $s_{e,h}=m_{e,h}/(m_e+m_h)$, where m_e and m_h are the effective electron and hole masses, respectively, and P is the momentum matrix element defined as $\langle X\,|\,P_x\,|\,S\rangle=-iP$. The function $F(\omega_L)$ is

$$F(\omega_L)=\left[\left[\frac{\hbar\omega_L-E_g+i\eta}{\hbar\Omega_{LO}}\right]^{1/2}-\left[\frac{\hbar\omega_S-E_g+i\eta}{\hbar\Omega_{LO}}\right]^{1/2}\right]^3, \tag{16}$$

with the convention that the imaginary parts of the square roots are positive. E_g is the gap energy, in our case $E_0+\Delta_0$.

The function $F(\omega_L)$ is plotted in Fig. 5 and $|F(\omega_L)|^2$ is plotted in Fig. 6 (dashed line). Note that because $s_e-s_h<0$, both components of a_F are positive near the maximum of $|a_F|^2$, which occurs at $E_g+\hbar\Omega_{LO}/2$. The prefactors in Eq. (15) are somewhat different from other published expressions for the forbidden Raman tensor, which can be defined in many different ways. In Ref. 3, a Raman susceptibility $\chi'_{s,\alpha\alpha}$ is used, which is related to a_F by (cgs units)

$$a_F=\left[\frac{2v_cVM^*\Omega_{LO}}{\hbar}\right]^{1/2}\chi'_{s,\alpha\alpha}\ . \tag{17}$$

Note that in Ref. 3 the Fröhlich constant C_F is defined with the factor $V^{1/2}$ in the denominator. The factor $\frac{2}{3}$ multiplying P^2 appears after summing over all bands at the $E_0+\Delta_0$ gap. The unimportant replacement of $1/\omega_L\omega_S$ by $(1/\omega_L^2)(\omega_S/\omega_L)^{1/2}$ comes from the slightly different definition of the scattering efficiency in Eq. (5). Equation 2.222 of Ref. 3 is valid, provided that one uses our definition of C_F [Eq. (9)] divided by $V^{1/2}$ and multiplies by 2 to correct a computational error. Note that the difference between the heuristic and exact calculations of Ref. 3 is reduced to a factor of $\frac{3}{2}$.

B. Impurity-induced LO-phonon Raman scattering

In addition to the "intrinsic" intraband Fröhlich mechanism, Gogolin and Rashba[8] have proposed another source of forbidden LO-phonon Raman scattering which involves exciton-impurity interaction. A typical diagram is shown in Fig. 4(b). Here the exciton scatters twice, due to the electron-phonon and electron-impurity interaction, respectively. Hence we have a fourth-order process, and the question arises as to why should this scattering mechanism be of comparable intensity with the intrinsic forbidden scattering, which is a third-order process. The reasons are twofold. First, as can be seen in Eq. (15), forbidden scattering through the intraband Fröhlich mechanism is proportional to the phonon wave vector q. In the case of intrinsic scattering the phonon wave vector is

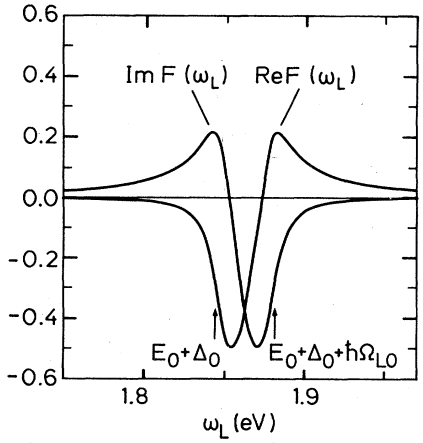

FIG. 5. Function $F(\omega_L)$ [Eq. (16)], which gives the frequency dependence of the Raman polarizability for intrinsic forbidden scattering. $E_g=1.844$ eV, $\eta=8$ meV, and $\hbar\Omega_{LO}=36.6$ meV.

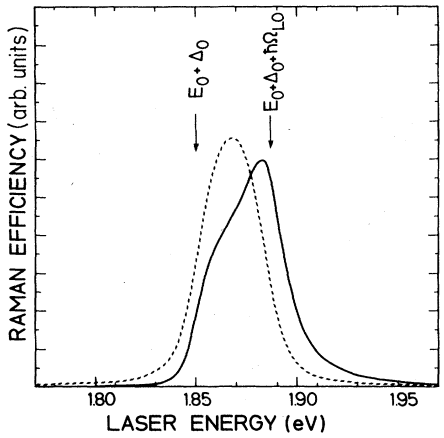

FIG. 6. Forbidden LO-phonon Raman scattering at the $E_0+\Delta_0$ gap of GaAs. Dashed line: intrinsic forbidden LO-phonon Raman scattering [$\propto |F(\omega_L)|^2$]. Solid line: impurity-induced forbidden LO-phonon Raman scattering [Eq. (A1)]. Parameters from Table I. The relative scale is arbitrary.

determined by wave-vector conservation and is very small. In the impurity-induced process, however, the quasi-momentum-conservation is relaxed and phonons with larger $\mathbf{q}$ vectors can participate in the Raman scattering. These larger $\mathbf{q}$ vectors greatly enhance the intraband Fröhlich contribution. On the other hand, whenever the phonon wave vector is not fixed by kinematics, double-resonance effects appear,[27] which again produce an enhancement of the Raman efficiency.

The first calculation of this impurity-induced process has been made by Gogolin and Rashba.[8] They calculate diagram 4(b) by considering only the ground state of the exciton,[9] and obtain the Raman tensor for $\hbar\omega_L > E_g$ by making some additional approximations to perform a final integral over the phonon wave vector. Their result does not allow us to elucidate the important issue of the position of the resonance maximum as a function of the laser frequency. Moreover, in the present case (GaAs at $E_0+\Delta_0$) we have a continuum of intermediate states which cannot be represented by a single level as in Ref. 8.

In view of the shortcomings of the early calculation, we have performed a new one by exploiting the similarities between impurity-induced and two-LO-phonon scattering.[28] The diagrams for this last process are very similar to Fig. 4(b), with the vertex H_{ei} replaced by $H_{e\mathrm{L}}$ and a second phonon being created. Several calculations of two-phonon scattering have been published,[27,29–31] that of Zeyher[29] being the easiest to adapt to the impurity case.

Two important approximations have been made at the outset: We assume the validity of the Born approximation and neglect multiple-impurity interference effects. This second assumption has been shown to lead to good results in the calculation of mobilities.[32] The Born approximation is not expected, in principle, to be appropriate for mobility calculations; nevertheless good agreement with experiments is often obtained.[33]

It was realized after performing the calculation that the position of the resonance maximum occurs for photon frequencies near the outgoing resonance, i.e., $\hbar\omega_L \approx E_g + \hbar\Omega_{\mathrm{LO}}$. We also found that the absolute values of the calculated Raman polarizability were not very different in the two cases studied: Scattering by neutral (hydrogenic) impurities and scattering via ionized impurities with a potential of the form

$$V(\mathbf{q}) = 4\pi e^2/[\epsilon_0(q^2+q_F^2)] ,$$

where $q_F = 2/\lambda$, λ being the mean distance between impurities. For impurity concentrations of the order 10^{14}–10^{15} cm^{-3}, $\lambda \sim 2000$ Å. Owing to double-resonance effects, the phonons which most contribute to the scattering efficiency have wave vectors $q_{\max} \cong 0.2/a_0$, where a_0 is the lattice constant. This means $q_{\max} \gg q_F$. Hence the final result is not very much affected by the parameter q_F, which only serves to eliminate unphysical divergences in the integration over $\mathbf{q}$. Moreover, for that value of $q_{\max}$, a hydrogenic impurity with Bohr radius $a_B \sim 100$ Å behaves almost like an ionized impurity, because the screening of the electron is reduced to 10% of the nuclear charge.[34] Therefore, one would not expect strong differences between the two model potentials used.

Details of the calculation are given in the Appendix. One obtains a diagonal tensor

$$\overleftrightarrow{R}_{Fi} = \begin{bmatrix} 1 & 0 & 0 \\ 0 & 1 & 0 \\ 0 & 0 & 1 \end{bmatrix} \alpha_{Fi} . \tag{18}$$

The final result for $|\alpha_{Fi}|^2$ is plotted in Fig. 6 (solid line). Of particular relevance for this work is the fact that impurity induced LO-phonon scattering resonates at *higher energies* than the intrinsic intraband Fröhlich scattering. The resonance peak is near $\hbar\omega_L = E_0+\Delta_0+\hbar\Omega_{\mathrm{LO}}$, i.e., $\hbar\omega_S \simeq E_0+\Delta_0$ (outgoing resonance), whereas in the intrinsic case it is exactly at $E_0+\Delta_0+\hbar\Omega_{\mathrm{LO}}/2$ (halfway between incoming and outgoing resonance).

C. Intrinsic versus extrinsic forbidden LO-phonon Raman scattering: Interference effects in both cases

Two possible sources of forbidden LO-phonon Raman scattering have been discussed in the preceding subsections. We would like to determine which of the two mechanisms prevails. We mentioned in Sec. I a possible procedure which has been successfully applied to CdS,[12] exploiting the $|q|$ dependence of the Raman polarizability [Eq. (15)]. In the case of III-V compounds, the problem of distinguishing between both scattering mechanisms has only been addressed by Trommer and Cardona,[11] who estimated the Raman efficiency for the intrinsic process.

Here we want to show how interference effects between allowed and intrinsic forbidden scattering lead to a determination of the proportion of intrinsic intraband Fröhlich scattering.

Since the Hamiltonians H_F and H_{DP} must be summed, we also must add the Raman tensors for intrinsic allowed and forbidden scattering before squaring in order to calculate the Raman efficiency. Adding Eq. (1) to Eq. (2), the tensor for backscattering at the (001) surface becomes

$$\overleftrightarrow{R}=\begin{bmatrix} a_F & a_{DP} & 0 \\ a_{DP} & a_F & 0 \\ 0 & 0 & a_F \end{bmatrix} . \quad (19)$$

Consequently, the Raman efficiency is proportional to the expressions given in Eqs. (3), and the interference between allowed and intrinsic forbidden scattering leads to different results for the configurations $z(x',x')\bar{z}$ and $z(y',y')\bar{z}$.

Let us now examine the case of extrinsic scattering induced by impurities. One would be tempted to add the corresponding tensor [Eq. (18)] to Eq. (19) before squaring. This would be *incorrect* in this case because the final states are different: Whereas in the intrinsic case one creates a single phonon with $q=|\mathbf{k}_L-\mathbf{k}_S|\approx 0.04/a_0$, the impurity-induced scattering is dominated by phonons with a much larger $\mathbf{q}$ ($q\approx 0.2/a_0$). The Raman efficiency is then proportional to

$$|a_F+a_{DP}|^2+|a_{Fi}|^2 \text{ for the } z(x',x')\bar{z} \text{ configuration}, \quad (20a)$$

$$|a_F-a_{DP}|^2+|a_{Fi}|^2 \text{ for the } z(y',y')\bar{z} \text{ configuration}, \quad (20b)$$

$$|a_F|^2+|a_{Fi}|^2 \text{ for the } z(x,x)\bar{z} \text{ configuration}. \quad (20c)$$

From a comparison of Eq. (20) with experiment, one can deduce the relative strengths of both forbidden mechanisms and compare them with the theoretical predictions of Eqs. (15) and (A1).

V. COMPARISON WITH EXPERIMENT

The results displayed in Fig. 2 show a difference between measurements in the $z(x',x')\bar{z}$ and $z(y',y')\bar{z}$ configurations. As we have seen, this can only occur if we have "intrinsic" forbidden LO-phonon Raman scattering. Hence we first try to explain our results with Eqs. (3). To that end we need an expression for the allowed polarizability a_{DP}. We use Eq. (14), adjusting the coefficients A_1, A_2, and A_3 to fit an independent measurement of the allowed LO-phonon Raman scattering in the configuration $z(x,y)\bar{z}$. We use $A_1/A_3=-1.4$, $A_2/A_3=-5.0$

Having determined a_{DP}, we now fit our forbidden LO-phonon Raman scattering [configuration $z(x,x)\bar{z}$] with an expression proportional to the function $|F(\omega_L)|^2$ in Eq. (16). With the two tensors a_{DP} and a_F, we can next calculate the interference effects according to Eq. (3). The results are shown in Fig. 7. See that, because $s_e-s_h<0$, the real and imaginary parts of a_F are *positive* near the resonance maximum. The allowed Raman scattering tensor is also positive, i.e., the interference is *constructive* for the $z(x',x')\bar{z}$ configuration, and destructive for the $z(y',y')\bar{z}$ configuration, in agreement with experiment. It should be mentioned here that the sign of the interferences depends on the sign of e_T, which has been assumed to be positive on the cation. These experiments may thus be viewed as confirming this sign of e_T.

The curves shown in Fig. 7 reproduce qualitatively the experimental ones. There are, however, some important quantitative differences:

(a) the observed interference is weaker than the calculated one;

(b) the point of maximum interference effect in the experimental curve is shifted towards lower energies with respect to the maximum of the forbidden Raman scattering, a fact that is not reproduced in Fig. 7;

(c) to fit the forbidden LO-phonon resonance with Eq. (3), one has to use $\eta=20$ meV in Eq. (18). This value is too large. Aspnes and Studna[35] measured $\eta=(6\pm 2)$ meV at $T=4.2$ K, and Trommer and Cardona[11] obtained a good fit of the two-LO-phonon resonance with $\eta=14$ meV.

Most of the discrepancies can be removed by assuming that impurity-induced scattering is also present. This means that part of the forbidden scattering observed does not interfere with a_{DP}. Moreover, due to the shift of the impurity-induced resonance to higher energies (Fig. 6), we observe a larger apparent broadening of the forbidden resonance and a relative shift between its maximum and the point of maximum interference which is only determined by the "intrinsic" mechanism. We then try to fit the experimental curve with Eq. (20), taking the relative strength $|a_F/a_{Fi}|^2$ as a parameter. The best fit (Fig. 2) is obtained with $\eta=8$ meV, and

$$|a_F|^2_{max}=0.4\,|a_{Fi}|^2_{max}, \quad (21)$$

where the subscript "max" indicates that both quantities are evaluated at the frequencies for which they are maximum. The result means that only 30% of the total forbidden Raman scattering signal is due to the intrinsic intraband Fröhlich mechanism. Note that, as expected, the results for the commercial GaAs sample show a stronger forbidden LO-phonon Raman scattering together with a much weaker interference effect, as one would expect for a sample with a higher impurity concentration.

In the fit to Fig. 2 we have multiplied our theoretical curves by a scaling factor. However, once we have determined the proportion of intrinsic and extrinsic forbidden scattering, we can compare our absolute measurements with the predictions of Eqs. (15) and (A1). The GaAs parameters needed for the theoretical evaluation are listed in Table I.[36] Theoretical and experimental results for the

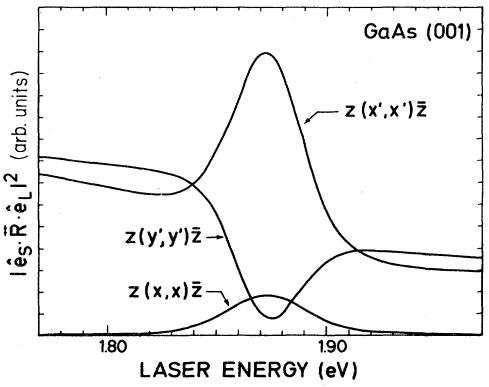

FIG. 7. Theoretical calculation of the interference profiles for Raman scattering after Eq. (3). See text for discussion.

TABLE I. Parameters used to evaluate the theoretical expressions of the Raman polarizability at the $E_0+\Delta_0$ gap of GaAs.

$E_g=1.844$ eV[a]	$m_e=0.0667m$[c]
$\eta=0.008$ eV[b]	$m_h=0.16m$[c]
$\Omega_{LO}=294$ cm^{-1}[c]	$\frac{2P^2}{3m}=13.9$ eV[d]
$M^*=6.58\times10^4$ m[c]	$q=7.25\times10^{-3}$ Å^{-1}[e]
$a_0=5.6534$ Å[c]	$x_F=0.06$[f]

[a] Reference 37.
[b] See Sec. V.
[c] Reference 38.
[d] Reference 36.
[e] $q=(n_L\omega_L+n_s\omega_s)/c$.
[f] See definition in Appendix.

TABLE II. Theoretical and experimental values of the Raman polarizability for intrinsic (α_F) and impurity-induced forbidden LO-phonon Raman scattering (α_{Fi}), evaluated at the resonance maximum.

	Theory	Experiment
$\lvert\alpha_F\rvert$ (Å^2)	11[a]	19[d]
$\lvert\alpha_{Fi}\rvert$ (Å^2)	4.1[b,c]	29[d]

[a] Equation (15).
[b] Equation (A1).

Raman polarizability are compared in Table II. The absolute theoretical values for the intrinsic forbidden scattering as well as the general shape of the interference are in quite good agreement with experiment. It is necessary to emphasize that in our calculation we neglect excitonic effects which are known to enhance dramatically the absolute values and to change the frequency dependence of the Raman polarizability.[26] Our results confirm that the excitonic interaction is not important near $E_0+\Delta_0$ at 100 K, although some residual effect could explain the somewhat lower theoretical values and the maximum in the configuration $z(y',y')\bar{z}$ at 1.88 eV (Fig. 2), which is not fully reproduced in our theory.

The fact that our purest sample presents 70% of impurity-induced scattering suggests that most of previous measurements on commercial samples are dominated by impurity effects. The theoretical absolute value obtained for the impurity-induced scattering, however, is smaller than the experimental one. This fact may be due to the approximations discussed in Sec. III, to the uncertainty in the number of impurities present, and/or to the strong dependence of this Raman polarizability on the broadening parameter η. This dependence is typical for second-order processes,[29] but is unimportant for first-order Raman scattering whenever $\eta<\hbar\Omega_{LO}$, as is the case in GaAs near the $E_0+\Delta_0$ gap. Our conclusion concerning the relative importance of the impurity-scattering mechanism can also be applied to the CdS case. The scattering efficiency measured in Ref. 12 for forward and backward scattering differs only by a factor of 2 and not by orders of magnitude as would be the case if only intrinsic q-dependent scattering were present.

ACKNOWLEDGMENTS

The technical assistance of M. Siemers, H. Hirt, and P. Wurster is gratefully acknowledged. We also want to thank E. Kisela for sample preparation and E. Bauser and B. Kunath for providing the liquid-phase-epitaxy sample.

APPENDIX

With the approximations discussed in Sec. IV, the calculation of impurity-induced LO-phonon Raman scattering becomes formally similar to the two-phonon scattering problem. In the case of LO phonons, the dominant contribution is given by an iteration of the Fröhlich Hamiltonian, Eq. (8). Zeyher[29] has calculated this effect by assuming free—electron-hole pairs and using a Green's-function technique to sum over the intermediate states. The impurity calculation is similar to that of Ref. 29, but one has to replace in a vertex the electron-phonon by the electron-impurity Hamiltonian, i.e., we have a factor $(C_F/q)^2$ in the two-phonon scattering which becomes

$$\left[\frac{C_F}{q}\right]\frac{4\pi e^2}{\epsilon_0(q^2+q_F^2)}$$

in the impurity case. On the other hand, terms arising from the permutation of the two Hamiltonians are *different* in the impurity calculation. The equivalent permutation merely leads to a factor of 2 in the two-phonon process. Using our definition of the Raman polarizability, the final result is

$$\begin{aligned}|\alpha_{Fi}|^2=&\left[\frac{1}{8\pi^2}\right]^3\left[\frac{1}{\omega_L}\right]^4\left[\frac{\omega_L}{\omega_S}\right]\left[\frac{2M^*\Omega_{LO}}{\hbar}\right]\left[\frac{e^2}{m}\right]^4\left[\frac{2P^2}{3}\right]^2\left[\frac{C_F}{\epsilon_0}\right]^2 v_c n_c\frac{1}{(\hbar\Omega_{LO})^6(a^*)^3}\\
&\times\int_0^\infty\frac{dx}{(x^2+x_F^2)^2}\,|A(s_e x,-s_e x,x_1,x_2,x_3)+A(s_h x,-s_h x,x_1,x_2,x_3)\\
&-A(s_e x,s_h x,x_1,x_2,x_3)-A(s_h x,s_e x,x_1,x_2,x_3)\\
&+A(s_e x,-s_e x,x_1,x_2',x_3)+A(s_h x,-s_h x,x_1,x_2',x_3)\\
&-A(s_e x,s_h x,x_1,x_2',x_3)-A(s_h x,s_e x,x_1,x_2',x_3)|^2\,,\end{aligned}\tag{A1}$$

with $a^*=\hbar^2/[2\mu(\hbar\Omega_{\rm LO})]$, $x_i=a^*k_i$, $x_F=a^*q_F$, and

$$k_3=\left[\frac{2\mu}{\hbar^2}\right]^{1/2}(\hbar\omega+i\eta-E_g-\hbar\Omega_{\rm LO})^{1/2}\ ,\quad {\rm Im}k_3>0 \tag{A2}$$

$$k_2'=\left[\frac{2\mu}{\hbar^2}\right]^{1/2}\left[\hbar\omega+i\eta-E_g-\frac{\hbar^2(x/a^*)^2}{2(m_e+m_h)}\right]^{1/2}\ ,\quad {\rm Im}k_2>0\ . \tag{A3}$$

n_c is the impurity concentration. All other quantities have the same definition as in Ref. 29.

[1]R. C. C. Leite and S. P. S. Porto, Phys. Rev. Lett. **17**, 10 (1966).

[2]A. Pinczuk and E. Burstein, Phys. Rev. Lett. **21**, 1073 (1968).

[3]M. Cardona, in *Light Scattering in Solids II,* edited by M. Cardona (Springer, Heidelberg, 1982), p. 19.

[4]W. Richter, in *Solid State Physics,* Vol. 78 of *Springer Tracts in Modern Physics,* edited by G. Höhler (Springer, Heidelberg, 1976), p. 121.

[5]D. C. Hamilton, Phys. Rev. **188**, 1221 (1969).

[6]R. M. Martin and T. C. Damen, Phys. Rev. Lett. **26**, 86 (1971).

[7]P. J. Colwell and M. V. Klein, Solid State Commun. **8**, 2095 (1970).

[8]A. A. Gogolin and E. I. Rashba, in *Proceedings of the Thirteenth International Conference on the Physics of Semiconductors,* edited by F. G. Fermi (Tipografia Marves, Rome, 1976), p. 284; Solid State Commun. **19**, 1177 (1976).

[9]Throughout our work, the word "exciton" refers to free—electron-hole pairs, for which the Coulomb interaction between electron and hole has been neglected. However, we denote "excitonic effects" those related to the electron-hole interaction. Gogolin and Rashba use the word "exciton" for the interacting electron-hole pair. "Free" exciton means not bound to impurities.

[10]R. M. Martin, Phys. Rev. B **4**, 3676 (1971).

[11]R. Trommer and M. Cardona, Phys. Rev. B **17**, 1865 (1978).

[12]S. Permogorov and A. Reznitsky, Solid State Commun. **18**, 781 (1976).

[13]J. Menéndez and M. Cardona, Phys. Rev. Lett. **51**, 1297 (1983).

[14]The sample was grown and characterized by B. Kunath at the Max-Planck-Institut. The total impurity concentration was estimated from mobility data. See C. M. Wolfe, G. E. Stillman, and J. O. Dimmock, J. Appl. Phys. **41**, 504 (1970).

[15]H. A. Schell, Z. Metallkd. **48**, 158 (1957); H. C. Gatos and M. C. Larine, J. Electrochem. Soc. **107**, 433 (1960); Y. Tarui, Y. Komiya, and Y. Harada, *ibid.* **118**, 118 (1971).

[16]A. Compaan and H. J. Trodahl, Phys. Rev. B **29**, 793 (1984).

[17]J. Wagner and M. Cardona, Solid State Commun. **48**, 301 (1983).

[18]D. D. Sell and H. C. Casey, J. Appl. Phys. **45**, 800 (1974).

[19]M. D. Sturge, Phys. Rev. **127**, 768 (1962).

[20]W. C. Dash and R. Newman, Phys. Rev. **99**, 1151 (1955).

[21]D. E. Aspnes and A. A. Studna, Phys. Rev. B **27**, 985 (1983).

[22]P. Vogl, in *Physics of Nonlinear Transport in Semiconductors,* edited by D. K. Ferry, J. R. Barker, and C. Jacoboni (Plenum, New York, 1980).

[23]W. Pötz and P. Vogl, Phys. Rev. B **24**, 2025 (1981).

[24]M. H. Grimsditch, D. Olego, and M. Cardona, Phys. Rev. B **20**, 1758 (1979).

[25]M. Cardona, F. Cerdeira, and T. A. Fjeldly, Phys. Rev. B **10**, 3433 (1974).

[26]R. Zeyher, T. S. Ting, and J. L. Birman, Phys. Rev. B **10**, 1725 (1974).

[27]R. M. Martin, Phys. Rev. B **10**, 2620 (1974).

[28]A. A. Klochikhin and A. G. Plyuklin, Pis'ma Zh. Eksp. Teor. Fiz. **21**, 267 (1975) [JETP Lett. **21**, 122 (1975)].

[29]R. Zeyher, Phys. Rev. B **9**, 4439 (1974).

[30]A. A. Klochikhin, S. A. Permogorov, and A. N. Reznitskii, Zh. Eksp. Teor. Fiz. **71**, 2230 (1976) [Sov. Phys.—JETP **44**, 1176 (1976)].

[31]A. A. Abdumalikov and A. A. Klochikhin, Phys. Status Solidi B **80**, 43 (1977).

[32]J. R. Meyer and J. Bartoli, Phys. Rev. B **30**, 1026 (1984).

[33]D. L. Rode and S. Knight, Phys. Rev. B **3**, 2534 (1971).

[34]A. S. Davydov, *Quantum Mechanics* (Pergamon, Oxford, 1965), p. 416.

[35]D. E. Aspnes and A. A. Studna, Phys. Rev. B **7**, 4605 (1973).

[36]A recent review on semiconducting properties of GaAs can be found in J. S. Blakemore, J. Appl. Phys. **53**, R123 (1982).

[37]The value of $E_0+\Delta_0$ at 100 K can be estimated using the fit to the temperature dependence of the E_0 gap with Varshni's formula (Ref. 38) and the value of Δ_0 measured in Ref. 35. The result is $E_0+\Delta_0=(1.849\pm0.003)$ eV. We obtain a better fit of our Raman scattering data with $E_0+\Delta_0=1.844$ eV. Some laser heating of the sample could explain this discrepancy.

[38]*Landolt-Börnstein Tables,* edited by O. Madelung, H. Schulz, and H. Weiss (Springer, Berlin, 1982), Vol. III/17a, p. 218.